Received 7 July 2020; revised 8 August 2020; accepted 9 August 2020. Date of publication 12 August 2020; date of current version 4 September 2020.

Digital Object Identifier 10.1109/OJAP.2020.3016047

Efficient Analysis of Electromagnetic Scattering in Post-Wall Waveguides and Its Application to Optimization of Millimeter Wave Filters

ARKADI AKOPIAN[1], GUGA BURDULI[1], VAKHTANG JANDIERI[2,3] (Senior Member, IEEE), HIROSHI MAEDA[4], WONBIN HONG[5] (Senior Member, IEEE), AHMED ABDELMOTTALEB OMAR[5] (Member, IEEE), KIYOTOSHI YASUMOTO[6] (Life Fellow, IEEE), DOUGLAS H. WERNER[7] (Fellow, IEEE), AND DANIEL ERNI[2,3] (Member, IEEE)

1 Department of Electrical and Computer Engineering, Free University of Tbilisi, 0159 Tbilisi, Georgia
2 General and Theoretical Electrical Engineering (ATE), Faculty of Engineering, University of Duisburg-Essen, 47057 Duisburg, Germany
3 CENIDE–Center for Nanointegration Duisburg-Essen, 47048 Duisburg, Germany
4 Department of Information and Communication Engineering, Fukuoka Institute of Technology, Fukuoka 811-0295, Japan
5 Department of Electrical Engineering, Pohang University of Science and Technology (POSTECH), Pohang 37673, South Korea
6 Faculty of Information Science and Electrical Engineering, Kyushu University, Fukuoka 819-0395, Japan
7 Department of Electrical Engineering, Pennsylvania State University, University Park, PA 16802, USA

CORRESPONDING AUTHOR: V. JANDIERI (e-mail: vakhtang.jandieri@uni-due.de)

This work was supported by the Deutsche Forschungs-gemeinschaft (DFG, German Research Foundation)-TRR 196 MARIE under Grant 287022738 (project M03).

The authors acknowledge support by the Open Access Publication Fund of the University of Duisburg-Essen.

ABSTRACT Functional post-wall waveguides and waveguide based compact passive circuits – namely bandpass filters – that are formed by introducing additional metallic or dielectric posts inside the post-wall waveguide are analyzed. Scattering parameters (*S*-parameters) of the waveguide-based bandpass filters are calculated using the method of images combined with the lattice sums technique. The developed formulation is numerically very fast, hence it can be considered as one of the best-suited approaches for the analysis of multiple scattering in post-wall waveguides and for numerical structural optimization. A breeder genetic algorithm is employed as a global search heuristic in order to track down the optimal geometrical parameters for the introduced posts yielding a bandpass filter characteristic in the desired frequency bands. Comparison with other references validates the correctness and utility of our formalism. Different configurations for the specifications of post-wall waveguide-based bandpass filters are discussed.

INDEX TERMS Scattering, periodic structure, bandpass filter, breeder genetic algorithm, modal analysis, post-wall waveguide.

I. INTRODUCTION

NON-PLANAR devices such as rectangular waveguides developed more than 50 years ago are still continuing to play an important role in many of today's GHz circuits and systems. However, these old technologies cannot be used for circuit and system integration because of their bulky mechanical and non-planar nature. This problem becomes much more pronounced at higher frequencies such as the millimeter-wave range. Post-Wall Waveguide (PWW) structures represent a good alternative to conventional non-planar guiding devices [1]–[4]. They are formed by a periodic arrangement of metallic posts on both sides with respect to the guiding region. PWWs offer a promising architecture for integration into planar circuits that operate in the microwave and millimeter wave frequency range. Functional PWW-based passive circuits are realized by introducing specific arrangements of additional posts into the guiding structure. In our recent works, we have proposed a self-contained, rigorous and numerically fast full-wave formalism, which can efficiently analyze the spectral responses of PWWs (both the real and complex solutions) and waveguide-based passive circuits (i.e., filters) relying on the model of 2-D

electromagnetic crystals [5], [6]. Such PWW-based filters are studied utilizing the lattice sums technique presenting a highly efficient computational scheme not only for the analysis of electromagnetic scattering in PWWs but also it is perfectly suitable for the optimization of a wide class of mm-wave filters [7]. This becomes increasingly valuable especially in the context of highly compact integrated filter solutions for complex mm-wave or THz applications in, for example, massive MIMO radar-based material characterization [8]–[10]. The accuracy of our formalism has been validated based on a comparison with the boundary integral-resonant mode expansion (BI-RME) method [4] and a hybridization of method of moments with a cylindrical eigenfunction expansion [11]. Excellent agreement has been observed for several configurations within the entire frequency range [5], [6]. The method is briefly discussed in Section II.

In this manuscript, the fundamental role of the multiple scattering by several posts inside a PWW is investigated by making use of the lattice sum technique together with the optimization method of PWW-based filters, namely, how to choose the structural parameters in order to achieve the desired filter characteristics in a short amount of computation time. For the computer-guided filter design we are relying on a breeder Genetic Algorithm (GA), which has already proven to be efficient in tracking down high-quality solutions in the framework of numerical structural optimization, e.g., in dense integrated optics [8]. The proposed optimization scheme is easily applicable to design of PWW-based filter structure, as the forward solver [5] is computationally efficient. In contrast to deterministic optimizers, which usually require an initial starting topology, our probabilistic breeder GA is built on a randomly initialized population of potential PWW structures, where the latter then evolves to a set of solutions that becomes increasingly competent in regard to the given specifications. The optimized results for iris filters (relatively simple model having a symmetric configuration), based on our formalism and a novel calibrated space mapping (SM) optimization technique in conjunction with a mono-modal equivalent circuit (EC) model and Ansoft HFSS [12], are compared. Very good agreement between the EC model and our formalism for the S-parameters of 3-pole and 8-pole filters with iris windows has been achieved, which is further discussed in Section III. The S-parameters for two PWW-based bandpass filters with complex geometries are presented in Section III. Additionally, CST simulations have been carried out to compare the frequency response of the two filters. Numerical investigations have shown that our proposed method is about 25 times faster than CST (less than 0.01 second per frequency). Measured data for one realized millimeter-wave bandpass filter is also presented. The concluding remarks are given in Section IV.

II. FORMULATION OF THE PROBLEM

We begin by considering the original PWW, which is illustrated in Fig. 1(a). It is composed of periodically distributed

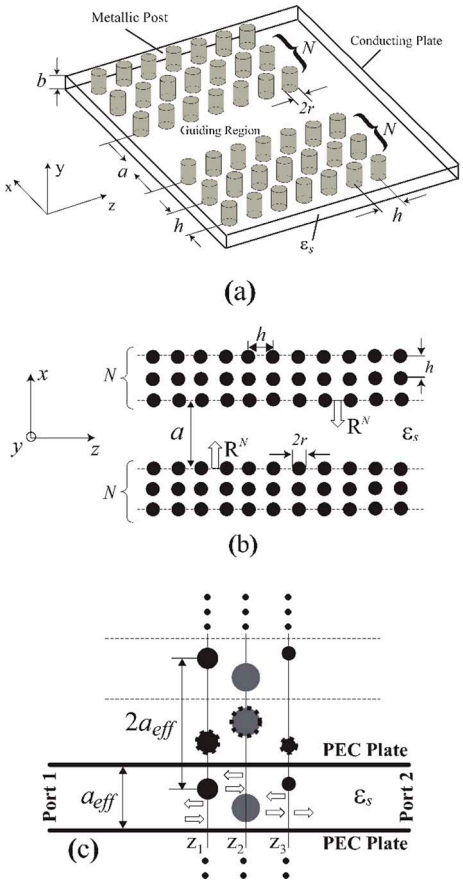

FIGURE 1. PWW with a square lattice bounded by an *N*-layered system of metallic rods (a); transversal view of a 2-D EBG structure to model the *N*-layered PWW (b); original posts in a rectangular PWW and their infinite number of images with respect to PEC walls (c).

conducting circular posts with a period h, thus, forming a lattice embedded in a dielectric substrate that connects two parallel conducting plates. Figure 1(a) shows the PWW structure formed by an N-layered square lattice. However, usually in case of metallic rods one layer ($N = 1$) is enough to strongly confine the power in the guiding region. The electromagnetic fields are uniform in the y-direction and the dominant mode TE_{10} is excited. This PWW can be considered as a 2-D electromagnetic bandgap (EBG) waveguide formed by parallel circular rods, which are infinitely extended in the y-direction [5], [6]. The 2-D EBG waveguide model is schematically depicted in Fig. 1(b). The complex wavenumber k_z at a fixed angular frequency ω can be calculated as follows:

$$\mathrm{Det}[\mathbf{I} \pm \mathbf{W}(k_{z0}, \omega)\mathbf{R}^N(k_{z0}, \omega)] = 0 \tag{1}$$

where $k_{z0} = \beta_0 + i\alpha, \beta_0$ and α are the phase and attenuation constants, respectively, $\mathbf{R}^N(k_{z0}, \omega)$ denotes the generalized reflection matrix of the multilayered periodic structure [13] calculated by the novel formalism developed in [14], $\mathbf{W}(k_{z0}, \omega)$ denotes the phase shift of each space-harmonic in the guiding region along the x-axis, $\mathbf{I}$ is the unit matrix and the signs "±" denote the odd and even

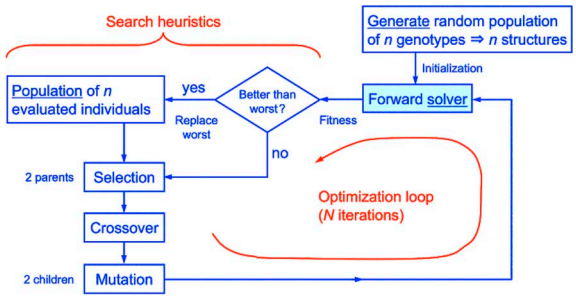

FIGURE 2. Schematic of the breeder GA's working principle.

modes, respectively. Accurate calculation of the generalized reflection matrix $\mathbf{R}^N(k_{z0}, \omega)$ is a challenging problem. Very recently, we succeeded in the development of an efficient method [14], which enables computation of the complex and leaky modes in a wide class of periodic waveguides for microwave and optical applications (see Appendix A). The advantage of the method is related to the fast and accurate calculation of the lattice sums – i.e., semi-infinite series of the cylindrical functions – in the case of complex wavenumbers.

Next, we employ an effective waveguide width a_{eff} that corresponds to the original PWW to create an equivalent rectangular waveguide structure [see Fig. 1(c)]. Usually, it is slightly smaller than the width a of the original PWW. Note that in our rigorous analysis the effective waveguide width $a_{eff}(\omega)$ is a function of frequency [5]. However, the detailed studies have shown that its variation is negligibly small, i.e., less than 3% over the entire frequency range. PWW filters are designed by carefully inserting multiple circular posts into the guiding region as depicted in Figs. 8 and 13. The virtual periodic array of parallel circular cylinders along the x-axis with a period of $2a_{eff}$ consists of two cylinders: the original post and its image with respect to the side wall [Fig. 1(c)]. Hence, the problem is reduced to a much simpler 2-D scattering problem by the infinite periodic structures (periodicity is along the x-axis) enabling the spectral responses of the filter transmission S_{21} (and reflection S_{11}) to be easily calculated (see Appendix B). Hence, the so-called forward problem, that is solved to achieve the filter responses, encompasses the described semi-analytical formalism in conjunction with the equivalent rectangular waveguide model where all introduced posts are efficiently processed using the method of images.

To setup structural optimization problem, the forward solver is then coupled to a global optimization algorithm, which in our case is a breeder GA [8], [15]. This class of population-based, probabilistic search heuristics relies on bio-inspired reproduction operators such as selection, crossover, and mutation, acting on the genotype of the filter structure (i.e., the parameter string) in order to (re)-produce corresponding successful phenotypes, namely optimal filter structures. The chosen breeder GA approach belongs to the class of steady-state GAs, where, contrary to standard generation-based implementations, implicit information on the potential progress is constantly present in the complete population. Breeder GAs have already proven very successful in different computer-guided device and system design scenarios [8], [15]. In addition, they offer the unique possibility to formally access this meta-information regarding the evolution process itself as well as the underlying features that qualify best performing solutions [8]. In the present optimization, we rely on a realistic scenario where a search is conducted for the number of the introduced posts, their radii, their material compositions and locations when the parameters of the original PWW are preliminarily defined. Note that the propagation and attenuation constants of the original PWW are also studied using the proposed self-contained formalism [14]. The quality of each solution is measured by the fitness function which is defined as following:

$$F = \left[\sum |\delta_k|^2 + \kappa\right]^{-1} \tag{2}$$

where κ is a small number included to avoid division by zero, $|\delta_k|^2$ is a positive definite residual, i.e., the square of the difference between the computed S_{21} and the target S_{21} (i.e., the filter specification) for each frequency sample k. The goal is to minimize this residual in the least-square sense within the analyzed frequency range. The schematic of the breeder GA's working principle is demonstrated in Fig. 2. The optimization with the breeder GA starts with a randomly generated population of fixed size. At each iteration (i.e., during evolution) the selection operator randomly chooses two parent strings according to a fitness proportional roulette-wheel scheme. Two offspring strings are then created using standard two-point crossover with subsequent mutation. After computing the fitness of the two offspring using our semi-analytical forward solver, these new individuals are introduced back into the population if their fitness is better than that of the two worst individuals in the population, which in this case are then removed. Hence, while iterating this reproduction cycle, a continuous flow of better performing individuals is migrating into the population at the expense of the worst performing ones, yielding a population that becomes increasingly performant with respect to the given specification.

III. NUMERICAL RESULTS AND DISCUSSIONS

In order to validate the correctness of the proposed formalism, the results are first compared with those based on a SM optimization method in conjunction with a mono-modal EC model and corresponding Ansoft HFSS simulations [12]. The results for 3-pole and 8-pole filters with iris windows using our method (solid line) and the SM technique (circles) are compared in Figs. 3 and 4, respectively. Very good agreement is observed within the entire frequency range. Although, in contrast to the SM approach, our method is based on a randomly initialized population, about 7 minutes and 15 minutes for 100 points are required to obtain the results shown in Figs. 3 and 4, respectively on a 3.8 GHz

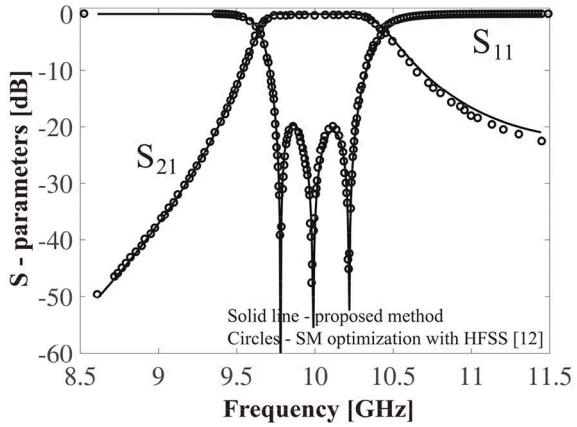

FIGURE 3. Magnitude of S-parameters for 3-pole filters with iris windows calculated using our proposed method (solid line) and the SM optimization technique in conjunction with the mono-modal equivalent circuit model and Ansoft HFSS simulations (circles) [12].

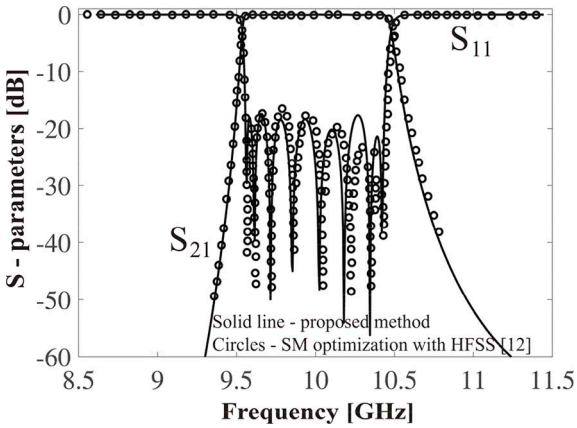

FIGURE 4. The same as in Fig. 3 but for 8-pole filters with iris windows.

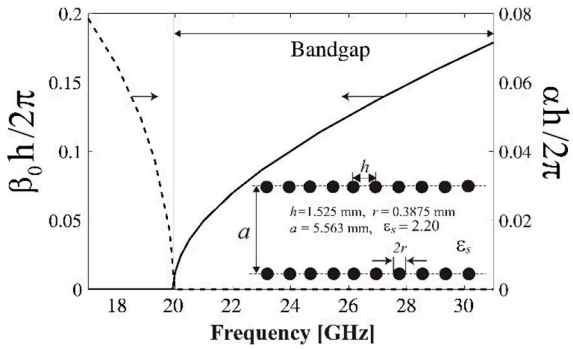

FIGURE 5. The propagation constant $\beta_0 h/2\pi$ and attenuation constant $\alpha h/2\pi$ of the PWW with the following structural parameters: $a = 5.563$ mm, $r = 0.3875$ mm, $h = 1.525$ mm, and $\varepsilon_s = 2.20$.

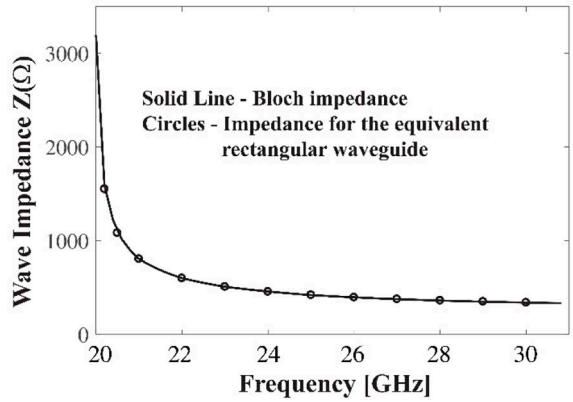

FIGURE 6. Characteristic wave impedance of the equivalent rectangular waveguide with $a_{eff} = 5.075$ mm (circles) and Bloch impedance of PWW (solid line). The structural parameters of the PWW are the same as those in Fig. 5.

Intel Core i7 CPU with 32 GB RAM (less than 0.01 second per frequency). Additionally, we note a fundamental difference between these two approaches: The SM optimization technique uses an efficient EC model to represent the optimized structural parameters when initial values are provided. Then, the commercial software package (Ansoft HFSS) is used to evaluate the S-parameters of the filters (only iris filters with relatively simple symmetric configuration have been considered in the literature). In comparison to the approximate SM technique, we propose a full-wave formalism, which calculates the S-parameters in a self-contained manner using the lattice sums technique. The method is applicable to the analysis of a wide class of EBG-based waveguides and filters operating from millimeter to optical frequencies.

Now that the efficiency of the full-wave formalism in conjunction with the breeder GA has been established, we apply it here to the optimization of two PWW-based bandpass filters with different specifications. In the first design example, we consider a PWW having a width $a = 5.563$ mm, a radius of the PEC cylindrical posts (as wall elements) of $r = 0.3875$ mm, a period of $h = 1.525$ mm and a relative dielectric permittivity of the substrate of $\varepsilon_s = 2.20$. In Fig. 5 the propagation constant $\beta_0 h/2\pi$ and the attenuation constant $\alpha h/2\pi$ (caused by the power leakage in the transverse direction) are plotted as a function of the frequency based on our self-contained method [14] (forward solver). The latter can be efficiently applied to the analysis of complex guided and leaky waves in a wide class of periodic and bandgap structures. The computation time to obtain the complex wavenumber per one frequency is about 0.07 seconds. The full-wave formalism proposed in [14] based on the lattice sums technique is highly efficient and provides a significant speedup over the standard approaches. The same formalism will be used for the filter designs presented here. Our analysis for the PWW has shown that the fundamental TE_{10} mode is well bounded and virtually lossless within the operating frequency range 20 GHz $< f <$ 31 GHz.

Next, using the theory of images, we define the effective width of the equivalent rectangular waveguide (Appendix B). The PWW's equivalent rectangular waveguide $a_{eff}(f)$, which has a weakly frequency dependent effective width [5], [6], is well approximated by the constant $a_{eff} = 5.075$ mm. The characteristic wave impedance Z of the equivalent rectangular waveguide (circles) and Bloch impedance of the original PWW (solid line) are shown in Fig. 6 [16], [17]. Without loss of generality, we choose a simple design goal namely

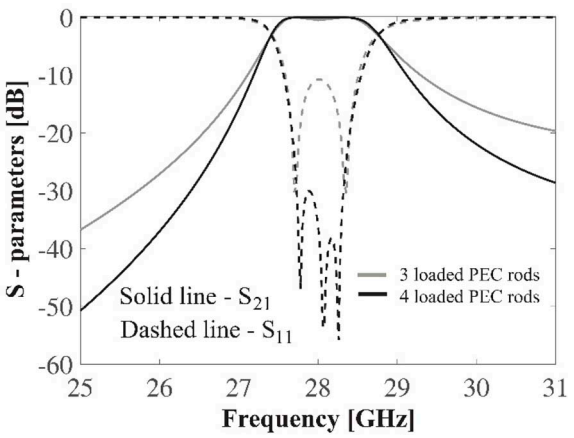

FIGURE 7. First design example: Frequency response (magnitude of S-parameters) of two optimized PWW-based bandpass filter topologies. The bandpass filters are formed by placing 3 (grey line) and 4 (black line) PEC rods into the PWW, where the latter is parametrized as following: $a = 5.563$ mm, $r = 0.3875$ mm, $h = 1.525$ mm, and $\varepsilon_s = 2.20$.

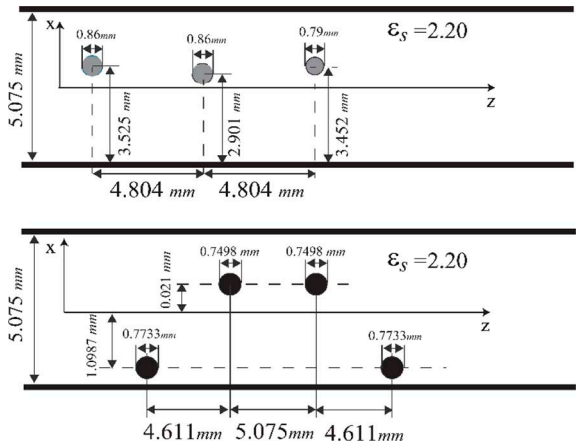

FIGURE 8. First design example: Optimized PWW bandpass filter topologies for three and four PEC cylindrical posts introduced into the equivalent rectangular waveguide having a width $a_{eff} = 5.075$ mm. The associated filter responses are shown in Fig. 7 using the same color code (i.e., grey and black curves).

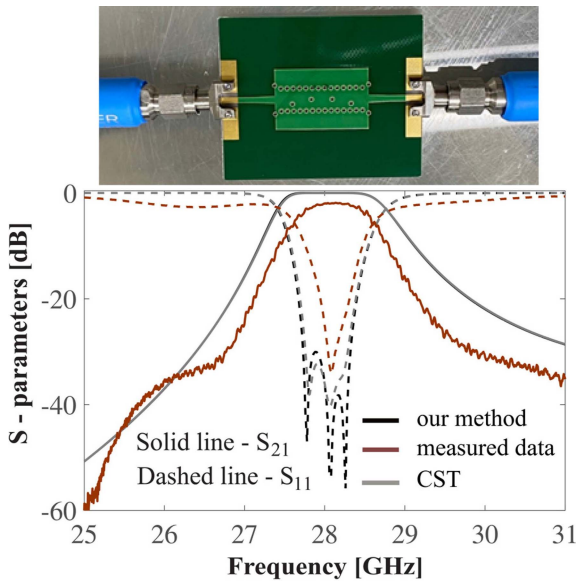

FIGURE 9. Photograph of the fabricated prototype and the frequency response (S - parameters) of the optimized PWW-based bandpass filter for four PEC cylindrical posts based on our method (black line), measurement (brown line), and CST (grey line). The structural parameters of the PWW are the same as in Fig. 7.

to realize a bandpass filter whose passband lies in the range 27.5 GHz $< f <$ 28.5 GHz with a minimal insertion loss of 0.1 dB. The subsequent breeder GA optimization encompasses a population of 50 individuals. The genotype of each individual has a size according to the number of posts under consideration for optimization multiplied by a 40-digit bit string, where each encodes the geometry of a corresponding filter structure. Optimized bandpass filter topologies are typically obtained after 2500 iterations, which translates into an overall optimization time of about 40 minutes. The filter responses, namely the frequency response of the scattering parameters S_{21} (solid line) and S_{11} (dashed line) for two optimized PWW-based bandpass filter designs with three (grey line) and four (black line) inserted PEC posts are presented in Fig. 7. The resulting passband ripple is about 0.18 dB yielding 3dB-bandwidths of 1.45 GHz and 1.3 GHz for filter realizations with three and four inserted posts, respectively. Figure 8 illustrates the optimized filter topologies, where the latter use a colour labelling that correspond to the associated filter responses as displayed in Fig. 7. Figure 9 depicts the frequency response of the S-parameters for the optimized bandpass filter with four loaded PEC cylindrical posts obtained using our method based on the lattice sums technique together with the theory of images (black line), experimental measurement (brown line) and CST (grey line). A photograph of the fabricated prototype is shown in Fig. 9. Taconic TLY 5 material with a dielectric constant of 2.2 and loss tangent equal to 0.0009 is used in the fabrication. The filter is fed by employing two 2.92 mm wave launcher connectors working from DC to 40 GHz. A transition from grounded coplanar waveguide to PWW is utilized to transfer the energy from the two ports to the filter with minimal reflection. The S-parameters of the fabricated filter were measured using a two-port Vector Network Analyzer KEYSIGHT N5224A. As for the computation time, we have calculated 100 points in the frequency range 25 GHz $<$ $f <$ 31 GHz versus 15 points using CST (note that CST is using fewer number of points to obtain similar results for the S-parameters). Although we are taking into account a larger number of points, our method is about 25 times faster than CST.

As a second design example, we consider a PWW having a width of $a = 6.0$ mm and cylindrical PEC posts as wall elements with radii $r = 0.25$ mm and a period of $h = 1.0$ mm, where the substrate medium has a higher relative permittivity of $\varepsilon_s = 2.32$. The width of the equivalent rectangular waveguide in this case was found to be $a_{eff} = 5.688$ mm. The propagation constant $\beta_0 h/2\pi$ and the attenuation constant $\alpha h/2\pi$ of the original PWW, as well as the characteristic wave impedance Z of the equivalent rectangular waveguide

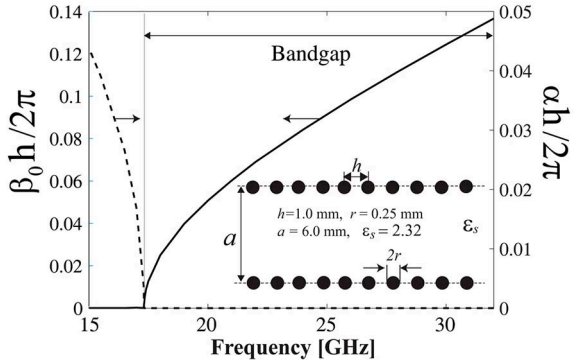

FIGURE 10. The propagation constant $\beta_0 h/2\pi$ and attenuation constant $\alpha h/2\pi$ of the PWW with the following structural parameters: $a = 6.0$ mm, $r = 0.25$ mm, $h = 1.0$ mm, and $\varepsilon_S = 2.32$.

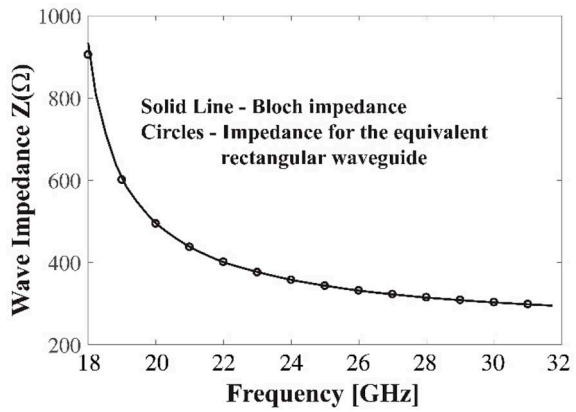

FIGURE 11. Characteristic wave impedance of the equivalent rectangular waveguide with $a_{eff} = 5.688$ mm (circles) and Bloch impedance of the PWW (solid line). The structural parameters of the PWW are the same as those in Fig. 10.

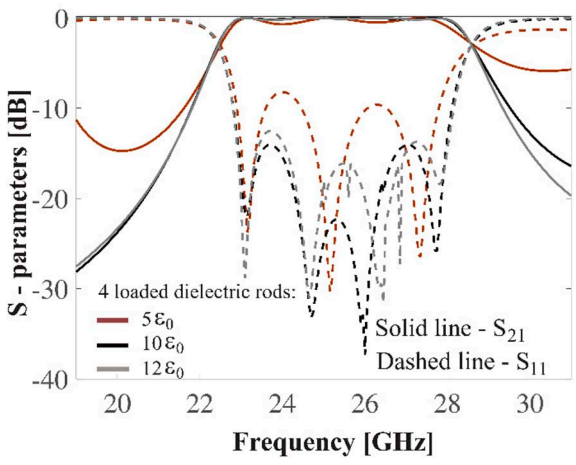

FIGURE 12. Second design example: Frequency response (magnitude of S-parameters) of three optimized PWW-based bandpass filter topologies. The bandpass filters are formed by placing 4 cylindrical posts made of the same dielectric materials with relative permittivity of 5 (brown line), 10 (black line) and 12 (grey line) into the PWW where the latter is parametrized as following: $a = 6.0$ mm, $r = 0.25$ mm, $h = 1.0$ mm and $\varepsilon_S = 2.32$.

and Bloch impedance, are shown in Figs. 10 and 11. The filter specifications now target a considerably larger passband between 22 GHz and 28 GHz. The frequency response of the

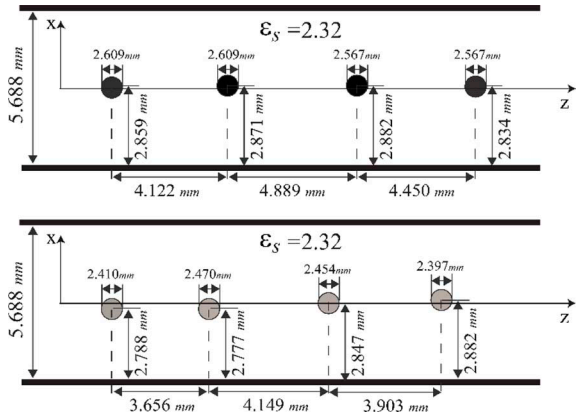

FIGURE 13. Second design example: Optimized PWW bandpass filter topologies for four cylindrical dielectric posts with a relative permittivity of (top) 10 and (bottom) 12 that are introduced into the equivalent rectangular waveguide having a width $a_{eff} = 5.688$ mm. The associated filter responses are shown in Fig. 12 labelled with the same color code (i.e., black and grey curves).

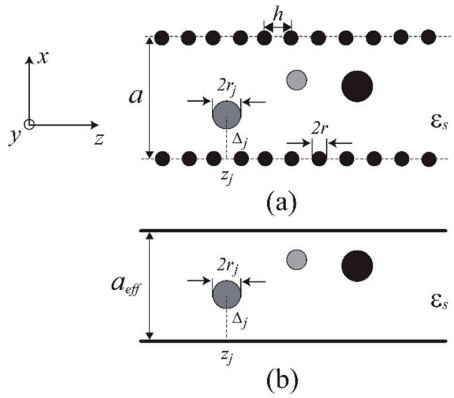

FIGURE 14. Top view of circular posts inserted into (a) a PWW and into (b) an equivalent rectangular waveguide with the effective width a_{eff}.

scattering parameters S_{21} (solid line) and S_{11}(dashed line) for the PWW-based bandpass filter designs – now using four dielectric posts with relative permittivities of 5 (brown line), 10 (black line) and 12 (grey line) – are illustrated in Fig. 12. Using our proposed formalism, about 10 minutes are required to obtain the results depicted in Fig. 12. Filter realizations with only three inserted dielectric posts lack the desired performance with respect to the given specifications. The achieved passband ripples with four dielectric posts having relative dielectric permittivities of 10 and 12 are estimated as 0.09 dB yielding 3dB-bandwidths around 6.8 GHz. Figure 13 depicts the optimized PWW-based bandpass filter topologies with four dielectric posts having relative permittivities of 10 and 12. These results are in a very good agreement with a symmetric filter prototype of similar extent as shown in [6, Fig. 6]. It is worth mentioning that with a proper material choice and corresponding spatial downscaling, such filter designs may also become accessible to the mm-wave and THz ranges.

IV. CONCLUSION

We reported on the first numerical structural optimization of PWW-based bandpass filters using a breeder genetic

algorithm in combination with our original self-contained semi-analytical formalism, which is applicable to the multiple scattering in a wide class of PWW configurations and PWW-based compact circuits. The optimization scenario is also apt to provide an insight into the underlying physics by revealing what actually qualifies as a promising filter topology with respect to the desired performance. The current research is focused on the analysis and design of PWW filter structures with finite electric conductivities and dielectric losses in order to deal with lossy scattering mechanisms within realistic filter structures [14], which is especially important for mm-wave up to THz frequencies.

APPENDIX A

The scattering process from each layer is described by the reflection and transmission matrices, which relate the set of the incident space harmonics to a set of reflected and transmitted ones. Reflection $\mathbf{R}_i(k_{z0}, \omega)$ and transmission $\mathbf{F}_i(k_{z0}, \omega)$ matrices for the i-th layer are derived as follows [13], [14]:

$$\mathbf{R}_i(k_{z0}, \omega) = \mathbf{U}^+(k_{z0})\big[\mathbf{I} - \mathbf{T}(k_s)\mathbf{L}(k_{z0}h, k_s h)\big]^{-1}\mathbf{T}(k_s)\mathbf{P}(k_{z0}) \tag{3}$$

$$\mathbf{F}_i(k_{z0}, \omega) = \mathbf{I} + \mathbf{U}^-(k_{z0})\big[\mathbf{I} - \mathbf{T}(k_s)\mathbf{L}(k_{z0}h, k_s h)\big]^{-1} \times \mathbf{T}(k_s)\mathbf{P}(k_{z0}) \tag{4}$$

with

$$\mathbf{P}(k_{z0}) = \left[i^s e^{is\cos^{-1}(k_{zq}/k_s)}\right] \tag{5}$$

$$\mathbf{U}^{\pm}(k_{z0}) = \left[\frac{2(-i)^s}{k_{xn}h} e^{\pm is\cos^{-1}(k_{zn}/k_s)}\right] \tag{6}$$

where $k_{xn} = \sqrt{k_s^2 - k_{zn}^2}$, $k_{zn} = k_{z0} + 2n\pi/h$, $k_{z0} = \beta_0 + i\alpha$, $k_s = \omega\sqrt{\varepsilon_s\varepsilon_0\mu_0}$, β_0 and α are the phase and attenuation constants, $\mathbf{P}(k_{z0})$ is a matrix that transforms the down-going q-th incident space harmonic wave into the s-th scattered cylindrical harmonic wave, $\mathbf{U}^+$ and $\mathbf{U}^-$ are the matrices that transform the s-th scattered cylindrical harmonic wave back to the up-going and down-going n-th space-harmonic waves (with $n, s, q = -M, -M+1, \ldots, 0, \ldots, M-1, M$), $\mathbf{T}(k_s)$ is the T-matrix of the isolated scatterer [13] and $\mathbf{L}(k_{z0}h, k_s h)$ is the matrix of the lattice sums. All the matrices in (3)-(6) are expressed as functions of the complex wavenumber k_{z0}, whereas the T-matrix does not depend on k_{z0}, but depends only on the geometrical and material parameters of the single cylinder as well as the background medium wavenumber k_s.

The matrix $\mathbf{L}(k_{z0}h, k_s h) = [L_{qs}]$ is a key element in our formalism. Each element L_m, with $m = q - s$, of the lattice sums is defined as:

$$L_m = \sum_{n=1}^{+\infty} H_m^{(1)}(k_s nh)\left[e^{ink_{z0}h} + (-1)^m e^{-ink_{z0}h}\right]$$
$$m = 0, 1, 2, \ldots \tag{7}$$

where $H_m^{(1)}$ is the m-th order Hankel function of the first kind. Recently we have used the formulation of the Ewald method to enable the fast and accurate calculation of the LSs in the case of complex-valued phase shifts k_{z0} [14]. The latter is a very fast method and is needed when analyzing complex guided and leaky waves. When the reflection and transmission matrices for the single-layered periodic structure of the circular rods is calculated, the generalized reflection matrix $\mathbf{R}^N(k_{z0}, \omega)$ can be easily obtained using a recursive algorithm [13], [14], [18].

APPENDIX B

As discussed in Section II we employ an effective waveguide width a_{eff} of the PWW to set up an equivalent rectangular waveguide structure as illustrated in Fig. 14(b). PWW filters are designed by carefully inserting multiple circular posts into the guiding region as depicted in Fig. 14(a). The j-th rod with radius r_j, whose center is at (Δ_j, z_j), is located within the equivalent rectangular waveguide. The excited TE_{m0} mode is expanded into cylindrical waves in the following form [19], [20]:

$$E_{y,m}^i = a_m^+ \sin(\kappa_m x)\exp(i\beta_m z) = \mathbf{\Phi}^T \cdot \mathbf{p}_m^+ \cdot a_m^+ \tag{8}$$

with

$$\mathbf{p}_m^+ = \left[p_{mn}^+\right],$$
$$p_{mn}^+ = \left[\frac{1}{2}(-i)^{n-1}\left\{\exp\left[i\left(n\theta_m - \kappa_m\Delta_j\right)\right] - (-1)^n\exp\left[-i\left(n\theta_m - \kappa_m\Delta_{\ j}\right)\right]\right\}\right] \tag{9}$$

$$\mathbf{\Phi} = \left[J_n\left(k_s\rho_0^+\right)\exp\left(in\phi_0^+\right)\right] \tag{10}$$

$$\cos\theta_m = \frac{\kappa_m}{k_s},\ \rho_0^+ = \sqrt{\left(x - \Delta_{\ j}\right)^2 + \left(z - z_j\right)^2}$$
$$\cos\phi_0^+ = \frac{x - \Delta_{\ j}}{\rho_0^+} \tag{11}$$

where $\kappa_m = \frac{m\pi}{a_{eff}}$, $\beta_m = \sqrt{k_s^2 - \kappa_m^2}$ is the propagation constant of the m-th mode along the z-axis, a_m^+ represents the amplitude of the incident field, J_n is the n-th order Bessel function of the first kind, and k_s is the wavenumber in the background material with a relative dielectric permittivity ε_s. Utilizing the theory of images [19], the scattered field is expressed in the following form:

$$E_y^s = \sum_{\ell=-\infty}^{\infty}\sum_{n=-\infty}^{\infty} X_n H_n^{(1)}\left(k_s\rho_\ell^+\right)\exp\left(in\phi_\ell^+\right) - \sum_{\ell=-\infty}^{\infty}\sum_{n=-\infty}^{\infty}(-1)^n X_n H_n^{(1)}\left(k_s\rho_\ell^-\right)\exp\left(-in\phi_\ell^+\right) \tag{12}$$

with

$$\rho_\ell^{\pm} = \sqrt{\left(x_\ell \mp \Delta_j\right)^2 + \left(z - z_j\right)^2},\quad \cos\phi_\ell^{\pm} = \frac{x_\ell \mp \Delta_{\ j}}{\rho_\ell^{\pm}} \tag{13}$$

where $x_\ell = x - 2a_{eff}\ell$, X_n are unknown amplitudes of the scattered multipole fields, and $(\rho_\ell^{\pm}, \phi_\ell^{\pm})$ denote the local polar coordinates with the origins at $(2a_{eff}\ell \pm \Delta_j, z_j)$.

The problem is reduced to a much simpler 2-D scattering problem by the periodic structures, which can be solved using the method presented in [14] and briefly summarized in Appendix A.

REFERENCES

[1] J. Hirokawa and M. Ando, "Single-layer feed waveguide consisting of posts for plane TEM wave excitation in parallel plates," *IEEE Trans. Antennas Propag.*, vol. 46, no. 5, pp. 625–630, May 1998.

[2] H. Uchiyama, T. Takenoshita, and M. Fujii, "Development of a 'laminated waveguide,'" *IEEE Trans. Microw. Theory Techn.*, vol. 46, no. 12, pp. 2438–2443, Dec. 1998.

[3] D. Deslandes and K. Wu, "Accurate modeling, wave mechanisms, and design considerations of a substrate integrated waveguide," *IEEE Trans. Microw. Theory Techn.*, vol. 54, no. 6, pp. 2516–2526, Jun. 2006.

[4] M. Bozzi, L. Perregrini, and K. Wu, "Modeling of conductor, dielectric and radiation losses in substrate integrated waveguide by the boundary integral-resonant mode expansion method," *IEEE Trans. Microw. Theory Techn.*, vol. 56, no. 12, pp. 3153–3161, Dec. 2008.

[5] V. Jandieri, H. Maeda, K. Yasumoto, and D. Erni, "Analysis of post-wall waveguides and circuits using a model of two-dimensional photonic crystals," *Progr. Electromagn. Res.*, vol. 56, pp. 91–100, Jun. 2017.

[6] K. Yasumoto, H. Maeda, and V. Jandieri, "Analysis of post-wall waveguides using a model of two-dimensional photonic crystal waveguides," in *Proc. IEEE Conf. Signal Process. Commun.*, Noida, India, Apr. 2015, pp. 74–79.

[7] MARIE—A collaborative research center on THz material characterization and localization funded by the Deutsche Forschungsgemeinschaft (DFG, German Research Foundation)—Project-ID 287022738—TRR 196 MARIE (Projects M03, M02).

[8] D. Erni *et al.*, "Application of evolutionary optimization algorithms in computational optics," *ACES J. Special Issue Genet. Algorithms*, vol. 15, pp. 43–60, Mar. 2000.

[9] J. Nagar and D. Werner, "Multiobjective optimization for electromagnetics and optics," *IEEE Antennas Propag. Mag.*, vol. 60, no. 6, pp. 58–71, Dec. 2018.

[10] R. Haupt and D. Werner, *Genetic Algorithms in Electromagnetics*. New York, NY, USA: Wiley, 2007.

[11] X. H. Wu and A. A. Kishk, "Hybrid of method of moments and cylindrical eigenfunction expansion to study substrate integrated waveguide circuits," *IEEE Trans. Microw. Theory Techn.*, vol. 56, no. 10, pp. 2270–2276, Oct. 2008.

[12] F. Mira, M. Bozzi, F. Giuppi, L. Perregrini, and A. Georgiadis, "Calibrated space-mapping approach for the design of SIW filters," in *Proc. 40th Eur. Microw. Conf.*, Paris, France, Sep. 2010, pp. 365–368.

[13] K. Yasumoto, Ed., *Electromagnetic Theory and Applications for Photonic Crystals*. Boca Raton, FL, USA: CRC Press, 2005, ch. 3.

[14] V. Jandieri, P. Baccarelli, G. Valerio, and G. Schettini, "1-D periodic lattice sums for complex and leaky waves in 2-D structures using higher-order Ewald formulation," *IEEE Trans. Antennas Propag.*, vol. 67, no. 4, pp. 2364–2378, Apr. 2019.

[15] C. Hafner, J. Smajic, and D. Erni, "Handbook of theoretical and computational nanotechnology," in *Simulation and Optimization of Composite Doped Metamaterials*, vol. 8, M. Rieth and W. Schommers, Eds. Stevenson Ranch, CA, USA: Amer. Sci., 2006, ch. 11, pp. 537–613.

[16] Q.-S. Wu and L. Zhu, "Numerical de-embedding of effective wave impedances of substrate integrated waveguide with varied via-to-via spacings," *IEEE Microw. Wireless Compon. Lett.*, vol. 26, no. 1, pp. 1–3, Jan. 2016.

[17] Z. Liu, L. Zhu, G. Xiao, and Z. Wu, "An effective approach to deembed the complex propagation constant of half-mode SIW and its application," *IEEE Trans. Compon. Packag. Manuf. Technol.*, vol. 6, no. 1, pp. 109–116, Jan. 2016.

[18] V. Jandieri and K. Yasumoto, "Electromagnetic scattering by layered cylindrical arrays of circular rods," *IEEE Trans. Antennas Propag.*, vol. 59, no. 6, pp. 2437–2441, Jun. 2011.

[19] K. Yasumoto, N. Koike, H. Jia, and B. Gupta, "Analysis of electromagnetic bandgap based filters in a rectangular waveguide," *IEICE Trans. Electron.*, vol. E89-C, no. 9, pp. 1324–1329, 2006.

[20] A. Akopian *et al.*, "Numerical study and optimization of post-wall waveguides and filters for millimeter waves," in *Proc. German Microw. Conf.*, Cottbus, Germany, Mar. 2020, pp. 212–215.